A novel hydrophobic carborane-hybrid microporous material for reversed C_2H_6 adsorption and efficient C_2H_4/C_2H_6 separation under humid conditions

Lingyao Wang,[#] Shuangshuang Wu,[#] Jianbo Hu,[#] Yunjia Jiang, Jiahao Li, Yongqi Hu, Yan Han, Teng Ben, Banglin Chen, Yuanbin Zhang*

[a]	Prof. L. Wang, S. Wu, Y. Jiang, J. Li, Y. Hu, Y. Han, Prof. Y. He, Prof. B. Chen, Prof. Y. Zhang, Key Laboratory of the Ministry of Education for Advanced Catalysis Materials, College of Chemistry and Materials Sciences Zhejiang Normal University, Jinhua, 321004, P.R. China E-mail: ybzhang@zjnu.edu.cn
[b]	Prof. J. Hu, Zhejiang Lab, Hangzhou, 311100, China.
[c]	Prof. T. Ben, Institute of Advanced Fluorine-Containing Materials, Zhejiang Normal University, Jinhua, 321004, China
[d]	Prof. B. Chen Fujian Provincial Key Laboratory of Polymer Materials, College of Chemistry & Materials Science, Fujian Normal University, Fuzhou 350007, P. R. China.

[#] These authors have contributed equally to this work

I General Information and Procedures

Unless otherwise noted, all the reactions were performed under air without N_2 or Ar protection. All reagents were used as received without purification unless stated otherwise.

Chemicals: 1,4-diazabicyclo[2.2.2]octane (DABCO, $C_6H_{12}N_2$), 1,2-di(4-pyridyl)ethylene and $Cu(NO_3)_2 \cdot 3H_2O$ (99%) were purchased from Energy Chemical. 1,12-dicarba-*closo*-dodecaborane (99%) and $Na_2B_{12}H_{12}$ (99%) were purchased from Yuanli Technology Company without further purification. C_2H_6 (99.9%), C_2H_4 (99.9%), C_2H_2 (99.9%), N_2 (99.9999%), He (99.9999%), Ar (99.9999%), C_2H_4/C_2H_6 (10:90), $C_2H_2/C_2H_4/C_2H_6$ (1:90:9) were purchased from Datong Co., Ltd.

Synthetic Procedures

1. Synthesis of 1,12-dihydroxycarbonyl-1,12-dicarba-closo-dodecaborane:

1,12-dihydroxycarbonyl-1,12-dicarba-closo-dodecaborane was prepared according to the reported literature.[1] To 2 g (13.9 mmoles) of 1,12-dicarba-*closo*-dodecaborane (*p*-carborane), dissolved in 150 mL of dry diethyl ether and stirred at 0 °C, 1.6 M (35 mL, 56 mmoles) n-BuLi was added via syringe. The reaction mixture was then warmed to room temperature and reacted under reflex for 1.5 hours. The reaction then cooled to -78 °C utilizing dry-ice/acetone bath. Carbon dioxide gas was bubbled into the reaction mixture for an hour while stirring. Diethyl ether was concentrated and the white solid was stirred in 100 mL of 3 M hydrochloric acid. Precipitate was filtered and washed in the following order: chilled water, hexanes, chloroform. The product was obtained as white solid (2.81 g, 87%) and dried on vacuum overnight.

2. Preparation of ZNU-10:
In a 40 mL vial, 19.36 mg (0.08 mmol) of $Cu(NO_3)_2 \cdot 3H_2O$, 18.56 mg (0.08 mmol) of p-$C_2B_{10}H_{10}(COOH)_2$ and 4.48 mg (0.04 mmol) of 1,4-diazabicyclo[2.2.2]octane was dissolved in 4 mL of DMF, 4 mL of methanol, 20 μL of HNO_3 and 2 mL of aqueous solution. The vial was sealed after 10

min of sonication and the mixtures were reacted at 80 °C for 6 h to obtain greenish-blue single crystals of ZNU-10. The greenish-blue single crystals were collected by filtration, and washed with methanol (3 mL x 3). The above crystals were soaked in anhydrous methanol for storage after three times (3 x 8 h) of solvent exchange using anhydrous methanol. Before gas adsorption measurement, the as-synthesized ZNU-10 was activated by vacuum at room temperature for 2 h and then at 120 °C for 10 h to remove the methanol molecules completely.

3. Preparation of single crystals of ZNU-1: ZNU-1 was prepared according to the reported literature[2]. To a 4 mL long thin tube was added a 1 mL of aqueous solution with $[Na]_2[B_{12}H_{12}]$ (~ 2 mg) and $Cu[NO_3]_2 \cdot 3H_2O$ (~ 2 mg). 1 mL of MeOH/H$_2$O mixture was slowly layered above the solution, followed by a 1 mL of MeOH solution of 1,2-di(4-pyridyl)ethylene (4 mg). The tube was sealed and left undisturbed at 298 K. After ~1 week, violet single crystals suitable for X-ray diffraction analysis were obtained.

4. Bulky synthesis of ZNU-1: A mixture of $[Na]_2[B_{12}H_{12}]$ (225 mg, 1.2 mmol, 1.2 equiv) and $Cu[NO_3]_2 \cdot 3H_2O$ (242 mg, 1 mmol, 1 equiv) was dissolved in 10 mL of water in a 100 mL round bottom flask and heated to 35 °C. Then a MeOH (30 mL) solution of 1,2-di(4-pyridyl)ethylene (dpe) (364 mg, 2 mmol, 2 equiv) was slowly added to the above solution during string (500 rpm). Gray violet solid formed immidiately, and the suspension was stirred at 35 °C for another 48 h. The solid was then collected by filtration, washed by MeOH (10 mL), and soaked in anhydrous MeOH for storage.

Single-crystal X-ray diffraction studies were conducted on a BrukerAXS D8 VENTURE diffractometer equipped with a PHOTON-100/CMOS detector (GaKα, λ = 1.34139 Å). Indexing was performed using APEX2. Data integration and reduction were completed using SaintPlus 6.01. Absorption correction was performed by the multi-scan method implemented in SADABS. The space group was determined using

XPREP implemented in APEX2.1 The structure was solved with SHELXS-97 (direct methods) and refined on F2 (nonlinear least-squares method) with SHELXL-97 contained in APEX2, WinGX v1.70.01, and OLEX2 v1.1.5 program packages. All non-hydrogen atoms were refined anisotropically. The contribution of disordered solvent molecules was treated as diffuse using the Squeeze routine implemented in Platon.

Powder X-ray diffraction (PXRD) data were collected on a Bruker AXS D8-Advance diffractometer (Cu K$\alpha\lambda$ = 1.540598 Å) with an operating power of 40 KV, 30 mA and a scan speed of 1.0°/min. The range of 2θ was from 5° to 50°.

Thermal gravimetric analysis was performed on a TGA STA449 F503030226 instrument. Experiments were carried out using a platinum pan under nitrogen atmosphere which conducted by a flow rate of 60 mL/min nitrogen gas. The data were collected at the temperature range of 50 °C to 600 °C with a ramp of 10 °C /min.

The static water contact angle (WCA) was measured using an optical contact angle meter (Dongguan Sindin SDC-100, Shengding, Dongguan, China).

The gas adsorption equilibrium measurements were performed on the Builder SSA 7000 instrument. Before measurements, the sample of ZNU-10 was evacuated at 25 °C for 2 h firstly, and then at 120 °C for 12 h until the pressure dropped below 7 μmHg; the sample of ZNU-1 was evacuated at 75 ºC for 1 day until the pressure dropped below 7 μmHg. The sorption isotherms were collected at 77 K, 278, 298 and 308 K on activated samples. The experimental temperatures were controlled by liquid nitrogen bath (77 K) and water bath (278, 298 and 308 K), respectively.

The BET surface areas and the pore size distributions of ZNU-10 and ZNU-1 were calculated from N_2 adsorption isotherms (77 K) via ASiQwin software, and the pore size distributions were obtained by NLDFT methods in the software.

The water vapor adsorption equilibrium measurements were performed on the BeiShiDe DVS instrument.

Fitting of experimental data on pure component isotherms

$$q = \frac{q_{sat,A}b_A p}{1+b_A p} + \frac{q_{sat,B}b_B p}{1+b_B p} \tag{S1}$$

Here, P is the pressure of the bulk gas at equilibrium with the adsorbed phase (Pa), q is the adsorbed amount per mass of adsorbent (mol kg^{-1}), $q_{sat, A}$ and $q_{sat, B}$ are the saturation capacities of site A and B (mol kg^{-1}), b_A and b_B are the affinity coefficients of site A and B (Pa^{-1}). For single-site Langmuir model, $q_{B,sat} = 0$.

$$b_A = b_{A0}\exp\left(\frac{E_A}{RT}\right); \quad b_b = b_{B0}\exp\left(\frac{E_B}{RT}\right) \tag{S2}$$

In eq (S1), the Langmuir parameters b_A, b_B are both temperature dependent.

In eq (S2), E_A, E_B are the energy parameters associated with sites A and B, respectively.

The isosteric heat of adsorption, Q_{st}, is defined as

$$Q_{st} = -RT^2\left(\frac{\partial \ln p}{\partial T}\right)_q \tag{S3}$$

where the derivative in the right member of eq (S3) is determined at constant adsorbate loading, q. The calculations are based on the use of the Clausius-Clapeyron equation.

IAST calculations of adsorption selectivity and uptake capacities:

For screening MOFs for separation of binary mixtures of components 1 and 2, the adsorption selectivity, S_{ads}, is defined by

$$S_{ads} = \frac{q_1/q_2}{y_{10}/y_{20}} \qquad \text{(S4)}$$

In eq (S4), y_{10}, y_{20} are the mole fractions of the bulk gas phase mixture.

Breakthrough experiments

The breakthrough experiments were carried out in the home-made dynamic gas breakthrough equipment. The experiments were conducted using a stainless steel column (4.9 mm inner diameter × 100 mm length) . The weights of ZNU-10 packed in the columns after full complete activation were 1.1453. The column packed with ZNU-10 was first purged with a Ar flow (20 mL min^{-1}) for 12 h at 120 °C. The mixed gas of C_2H_4/C_2H_6 (v/v, 90/10) was then introduced with a flowrate of 2 mL min^{-1}. Outlet gas from the column was monitored using gas chromatography (GC-9860-5CNJ) with the thermal conductivity detector TCD. After the breakthrough experiment, the sample was regenerated with a Ar flow of 20 mL min^{-1}.

The illustration of the gas breakthrough equipment working mechanism is showing in Figure S22.

Density functional theory (DFT) calculations

The density functional theory (DFT) calculations were performed using Castep code. In all calculations, the generalized gradient approximation (GGA) with Perdew–Burke–Ernzerhof (PBE) exchange correlation were used. A semi-empirical addition of dispersive forces to conventional DFT was included in the calculation to account for van der Waals interactions. A cutoff energy of 544 eV and a $2 \times 2 \times 2$ k-point mesh (generated using the Monkhorst-Pack scheme) were found to be enough for the total energy to converge within 0.01 meV atom^{-1}. The structures and the atomic positions of ZNU-10 were first fully optimized. The guest gas molecules were then introduced into the optimized structure, followed by a full structural relaxation. The initial locations of gas molecules were obtained from the experimental SCXRD data. To

obtain the gas binding energy, an isolated gas molecule placed in a supercell (with the same cell dimensions as the MOF crystal) was also relaxed as a reference. The static binding energy (at T = 0 K) was then calculated using:

$$\Delta E = E_{\text{MOF}} + E_{\text{gas}} - E_{\text{MOF+gas}} \qquad \text{S5}$$

where E_{MOF} represents the energy of the empty MOF framework, E_{gas} and $E_{\text{MOF+gas}}$ represent the energy of isolated adsorbed molecule and adsorbed-MOF structure, respectively.

Grand canonical Monte Carlo (GCMC) simulations

Grand canonical Monte Carlo (GCMC) simulations were performed in MS 2017R2 package using sorption module. The Qeq charges for atoms of ZNU-10 were selected in GCMC simulations. The simulations adopted the locate task, Metropolis method in sorption module and the universal force field (UFF). During the simulation, the framework was considered to be rigid during the simulation and the interaction energy between the adsorbed molecules and the frameworks were computed through the Coulomb and Lennard-Jones 6-12 (LJ) potentials. The cutoff radius was chosen 12.5 Å for Van der Walls interaction and the long range electrostatic interactions were handled using the Ewald summation method. The loading steps and the equilibration steps were 1×10^7, the production steps were 1×10^7.

II Characterization
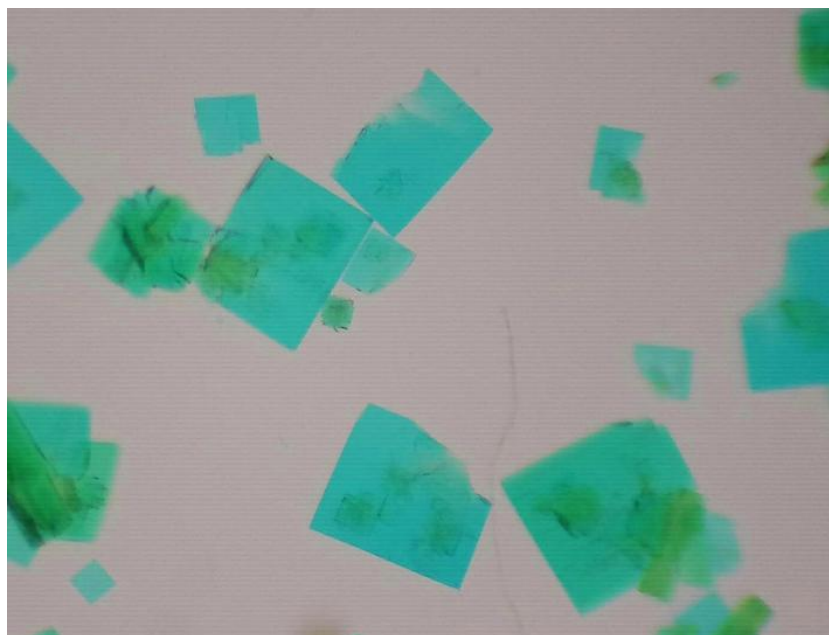
Figure S1. Photography of the single crystals of ZNU-10. From different directions we can see the green and blue colors of the single crystals.

add MeOH
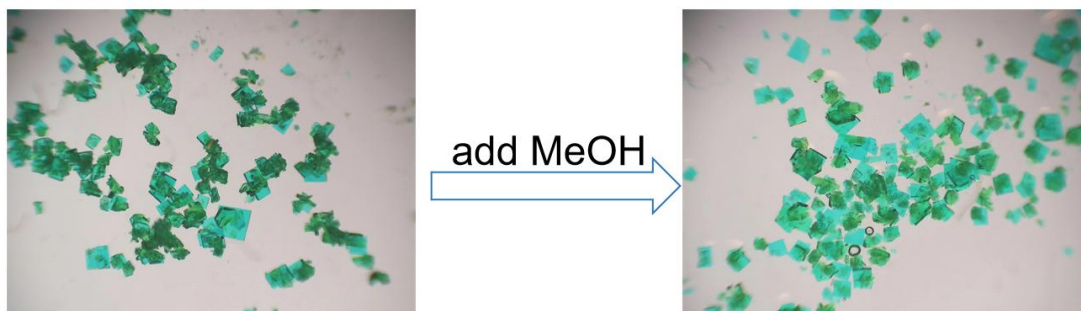
Humid air 3 months

Figure S2. Photograph of single crystals of ZNU-10 after exposure to humid air for 3 months and re-soaking into MeOH
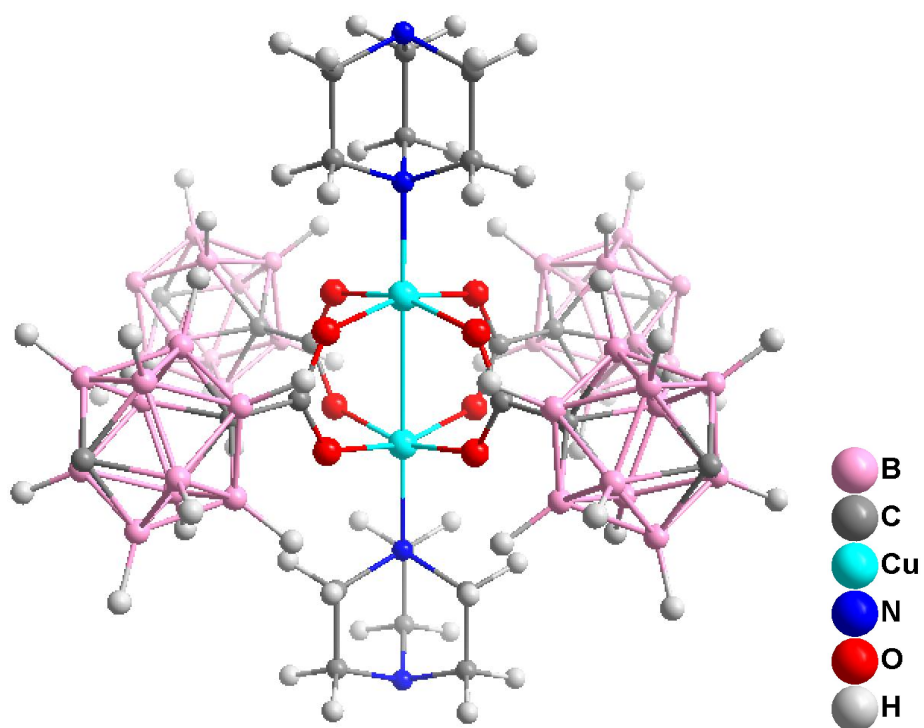
Figure S3. The typical Cu(II) coordination environment of ZNU-10 without open metal sites.
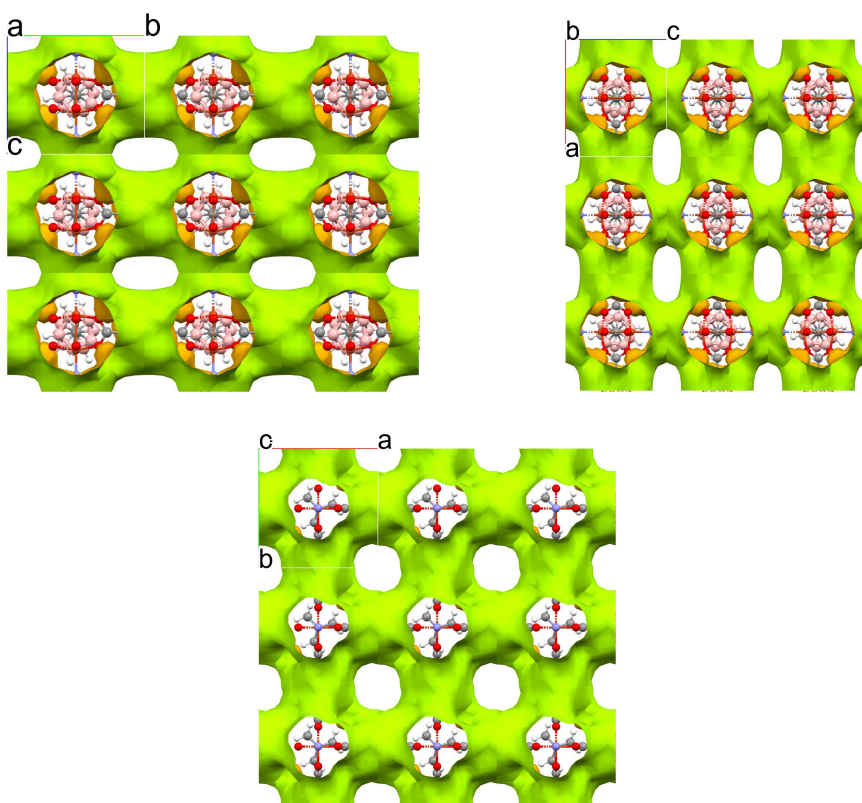
Figure S4. Void surface of ZNU-10 viewed down the crystallographic a-, b-, c-axis generated using a probe of 1.2 Å.
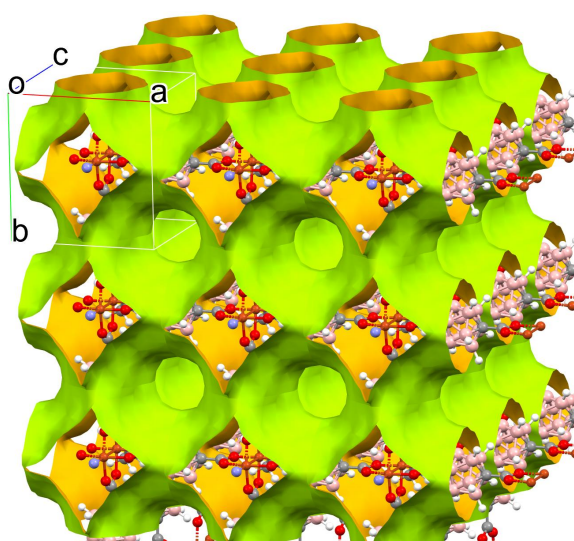
Figure S5. Void surface of ZNU-10 determined using a probe of 1.2 Å.
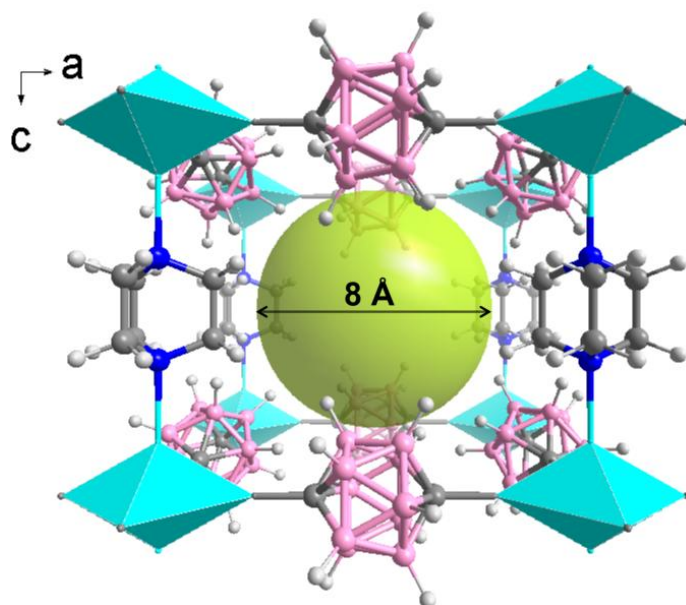
Figure S6. The micropore within ZNU-10. The micropore diameter is ~8 Å considering the van der Waals radius (1.2 Å) of hydrogen atoms in the pore surface. (the micropore is illustrated by a green sphere).

C-H···H-C = 12.45 Å
B-H···H-B = 10.07 Å
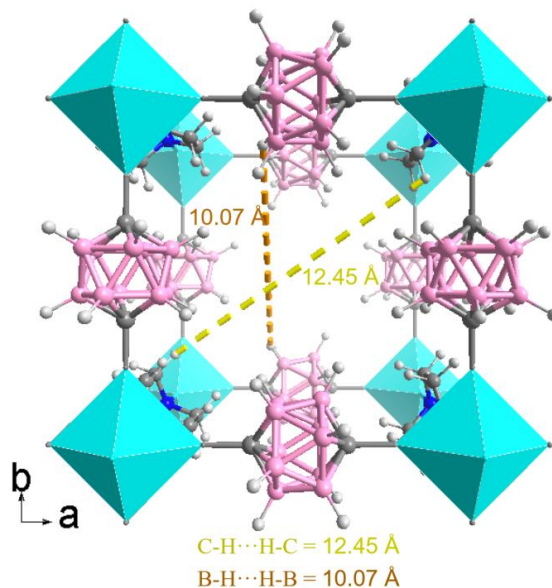
Figure S7. The distances between C-H···H-C and B-H···H-B within a single crystal unit cell in ZNU-10. After subtracting two an der Waals radii (1.2 Å), the micropore size can be considered in the range of 7.67-10.05 Å.

Table S1. Single crystal data of as synthesized ZNU-10, activated ZNU-10, C_2H_4@ZNU-10 and C_2H_6@ZNU-10

		As synthesized ZNU-10	Activated ZNU-10	C_2H_4@ZNU-10	C_2H_6@ZNU-10
cell	a (Å)	11.1145	11.1131	11.1145	11.1093
	b (Å)	11.1145	11.1131	11.1145	11.1093
	c (Å)	9.6132	9.6111	9.5867	9.5788
	α=β=γ	90°	90°	90°	90°
Volume (Å³)		1187.5	1187.0	1184.27	1182.2
Temperature		120 K	120 K	120 K	120 K
Space group		P-4m2	P-4m2	P-4m2	P-4m2
Hall group		P-4-2	P-4-2	P-4-2	P-4-2
Formula		$B_{10}C_7CuNO_4H_{16}$	$B_{10}C_7CuNO_4H_{16}$	$C_7H_{16}B_{10}CuNO_4$, 0.55(C_2H_4)	$C_7H_{16}B_{10}CuNO_4$, 0.7(C_2H_6)
MW		333.73	333.73	365.29	370.89
density		0.933	0.934	1.024	1.042
Data completeness		1.74/0.99	1.77/1.00	1.75/1.00	1.74/0.99
R		0.0447	0.0784	0.0474	0.0607
wR2		0.1249	0.2315	0.1231	0.1523
S		1.124	1.108	1.144	1.050
CCDC. No		2287884	2287885	2287887	2287888

Note: the single crystals of ZNU-10 are highly stable. The as-synthesized single crystal of ZNU-10 remained its crystallinity and quality over several months in ambient conditions with humidity. Besides, the activated single crystal of ZNU-10 remained its crystallinity and quality over 10 cycles of adsorption and desorption of hydrocarbons.
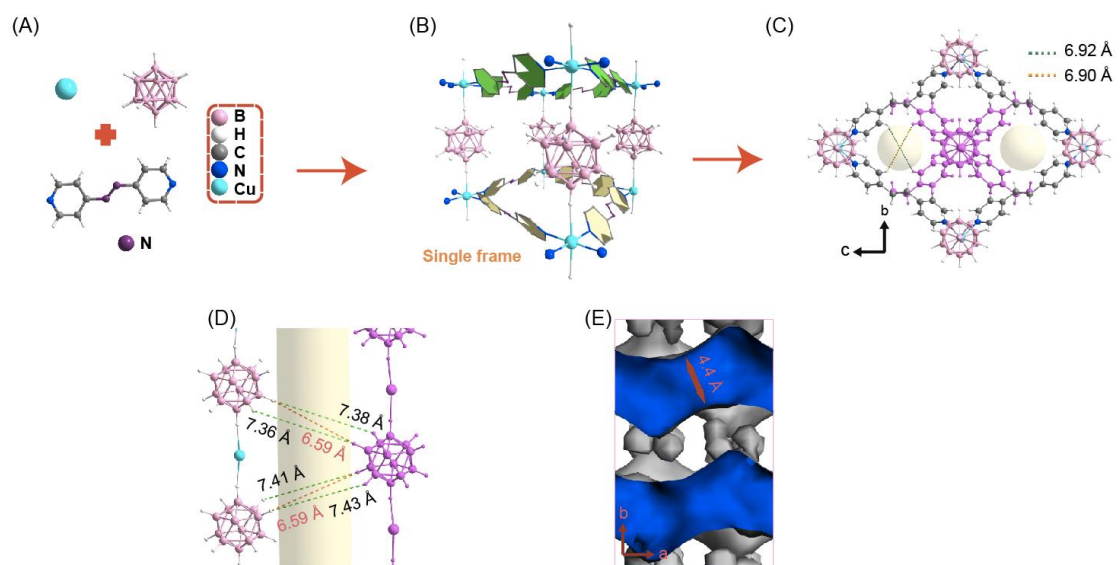
Figure S8. Porous structure of ZNU-1.
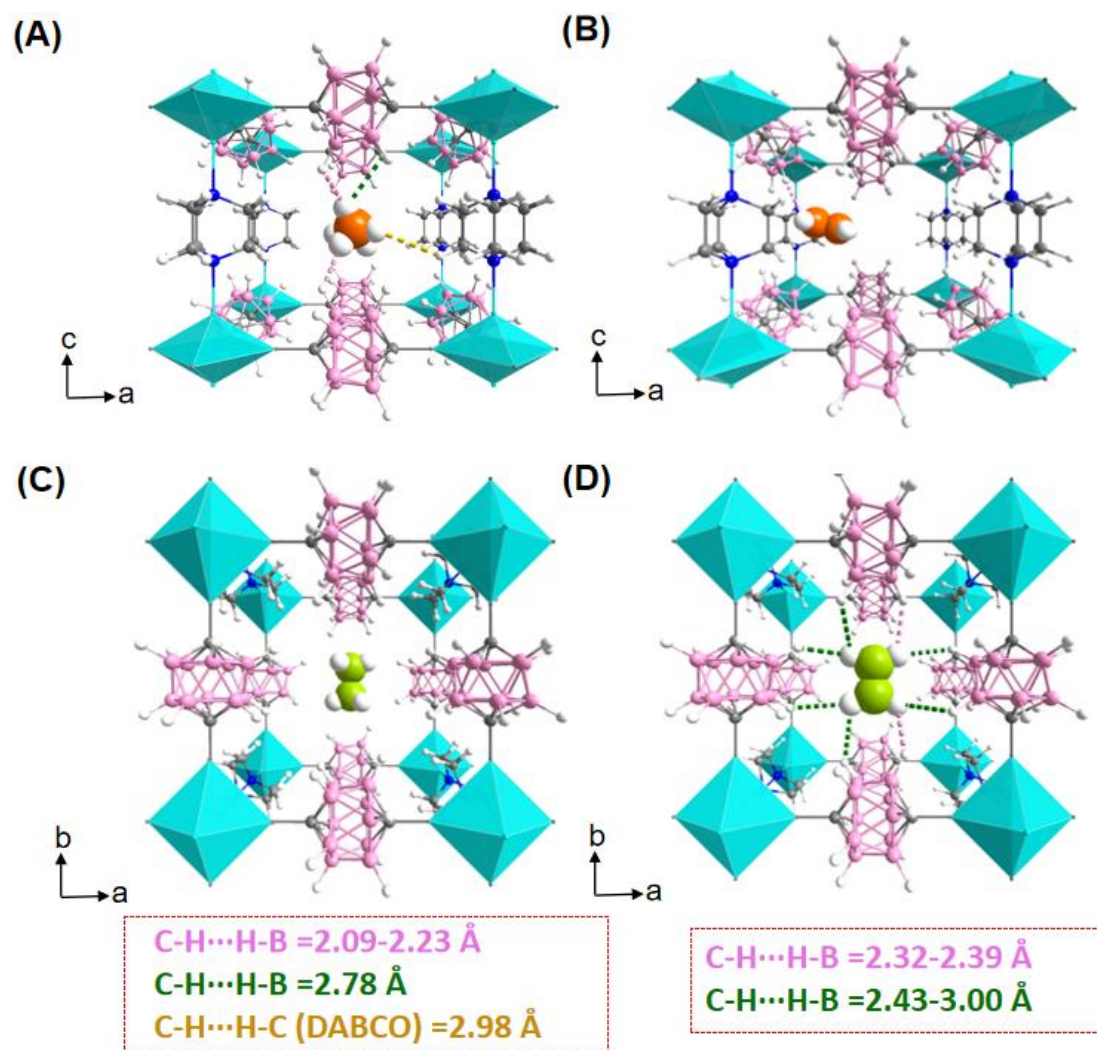
Figure S9. *In-situ* single crystal structure of C_2H_6@ZNU-10 (A, C) and C_2H_4@ZNU-10 (B, D) with two different adsorption sites. Different colors for hydrocarbons represent different binding sites.
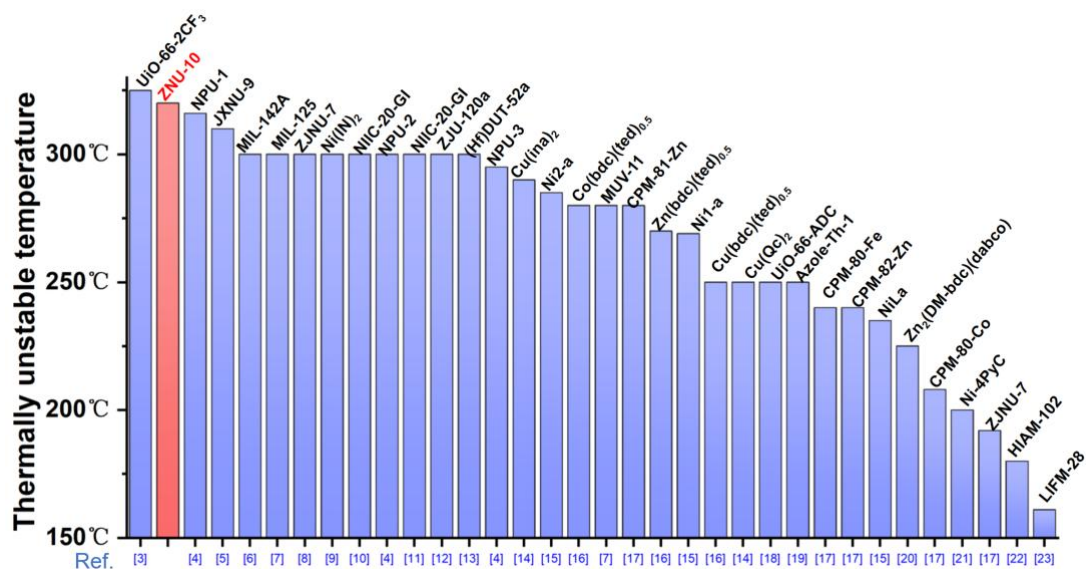
Figure S10. Comparison of the thermal stability in some previously reported C$_2$H$_6$-selective materials.
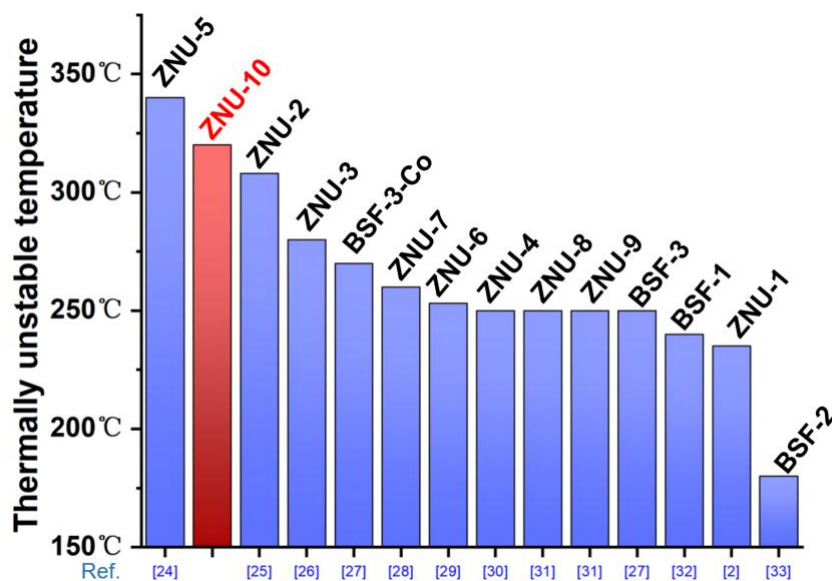
Figure S11. Comparison of the thermal stability in the boron cluster anion hybrid MOFs and Cu(II) based MOFs .

III Adsorption data
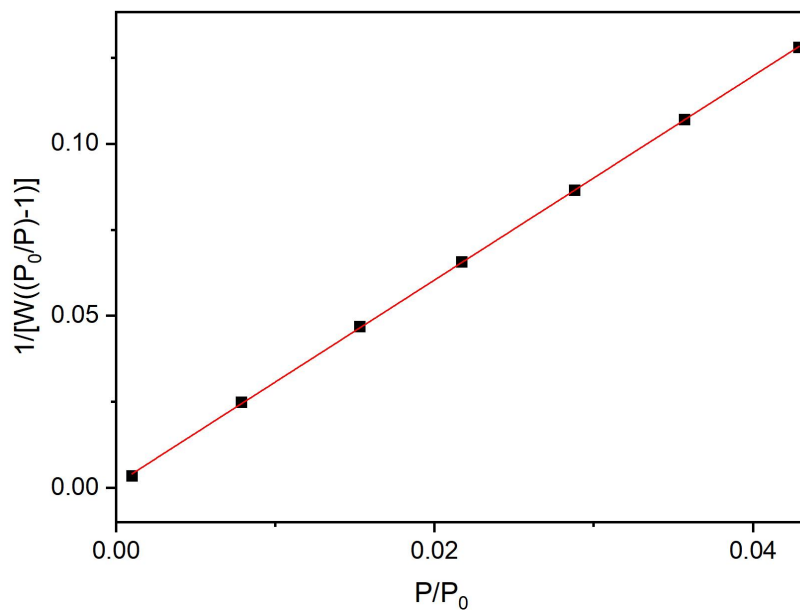
Figure S12. BET surface area fit for ZNU-10 from 77 K N_2 adsorption isotherm.

MBET summary:

Slope=2.972

Intercept=1.055×10^{-3}

Correlation coefficient, r=0.999973

C constant=2818.119

The BET surface area calculated from the N_2 adsorption isotherms under the pressure range of $P/P_0 = 0.001$-0.04 is 1171 m^2/g.

The total pore volume calculated from the N_2 adsorption isotherms is 0.454 cm^3/g .
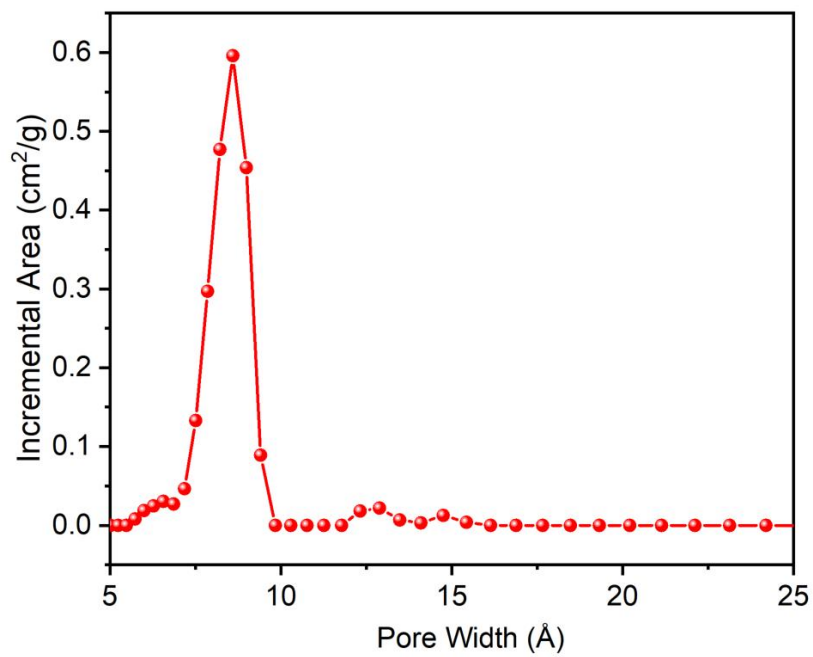
Figure S13. The calculated pore size distribution of ZNU-10.
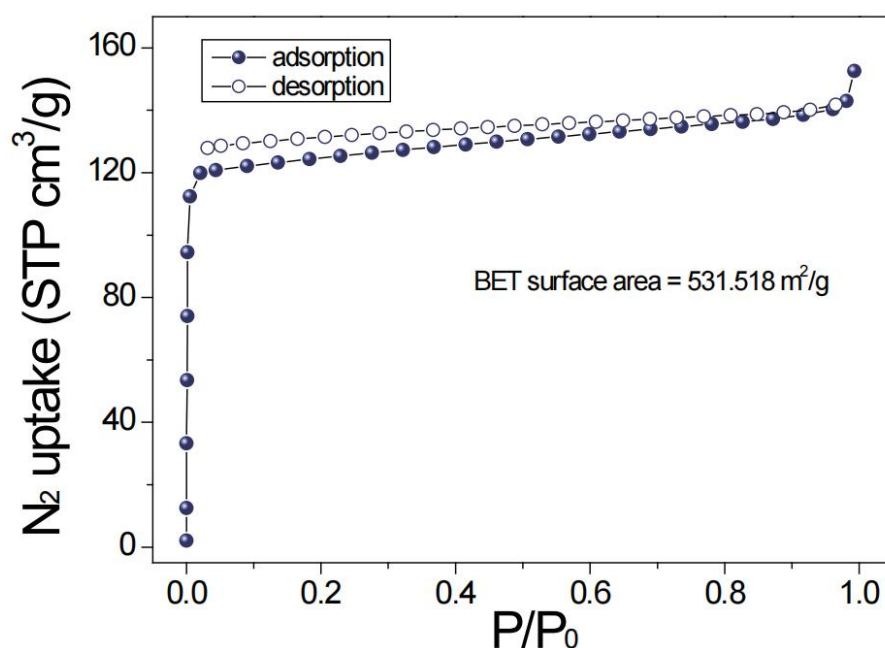
Figure S14. The sorption isotherm of N_2 on ZNU-1 at 77 K.

The BET surface area calculated from the N_2 adsorption isotherms under the pressure range of $P/P_0 = 0.0001\text{-}0.01$ (for ultramicropores) is 531. 518 m^2/g. Theoretical value: 545.198 m^2/g

MBET summary:

Slope = 6.547;

Intercept = 5.088×10^{-3};

Correlation coefficient, r= 0.999099;

C constant = 1287.866.

Table S2. Comparison of physicochemical parameters of C_2H_2, C_2H_4 and C_2H_6

Gas molecules		
Boiling point (K)	169.4	184.5
Kinetic diameter (Å)	4.16	4.44
Molecular dimensions (Å^3)	3.28×4.18×4.84	3.81×4.82×4.08
Polarizability×10^{25} (cm^{-3})	42.5	44.3
Quadrupole moment ×10^{26} (e.s.u. cm^2)	1.5	0.65
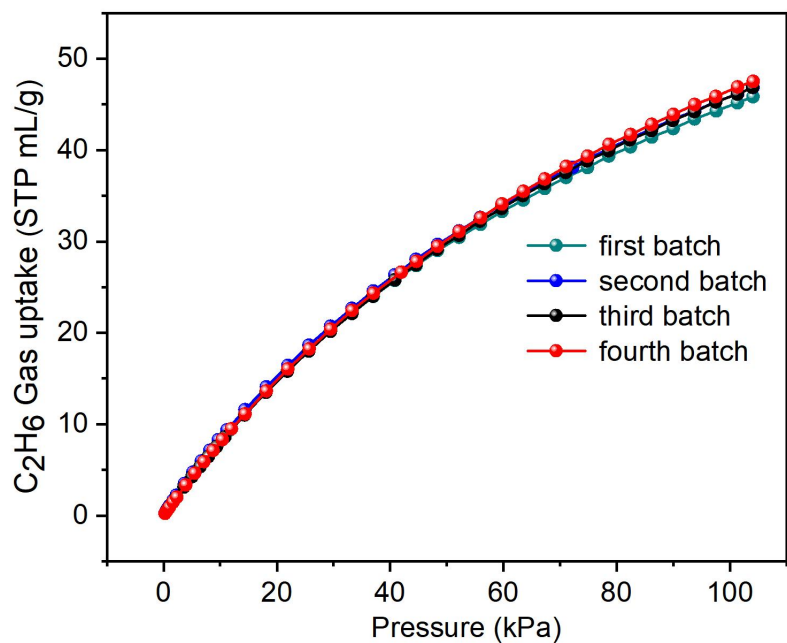
Figure S15. Different batches of C_2H_6 sorption measurements on ZNU-10 at 298 K from 0 to 1.0 bar.
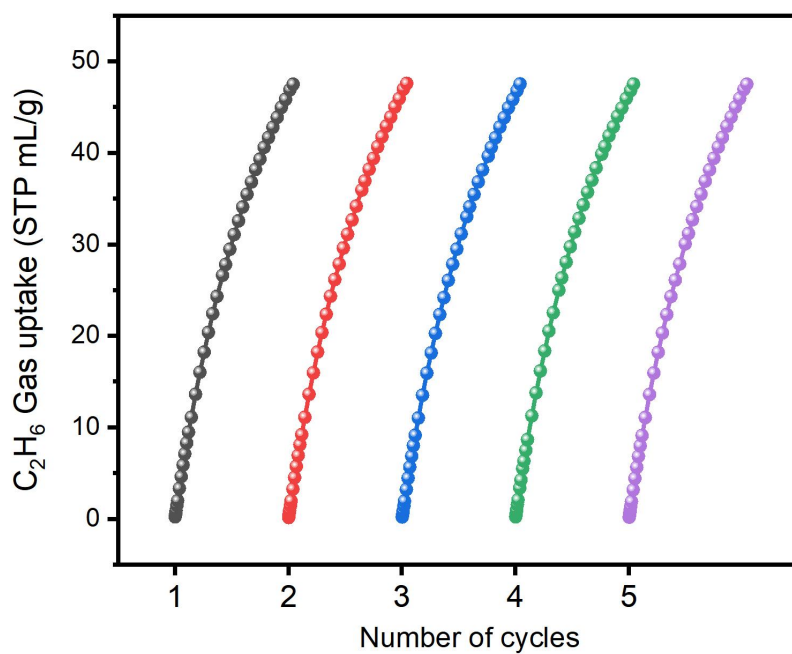
Figure S16. Cycling tests of C_2H_6 sorption measurements on ZNU-10 at 298 K from 0 to 1.0 bar.
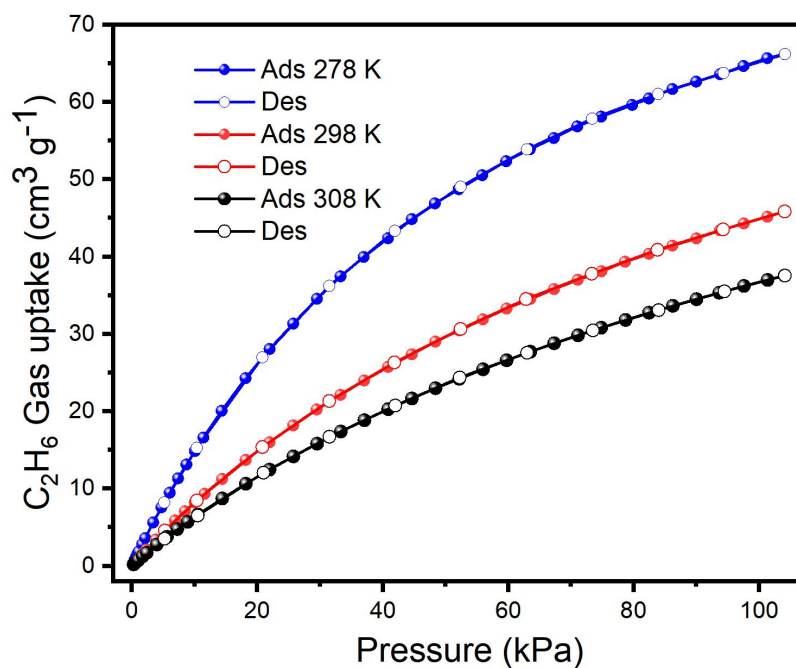
Figure S17. Adsorption and desorption isotherms of C_2H_6 on ZNU-10 at 278 K, 298 K and 308 K.
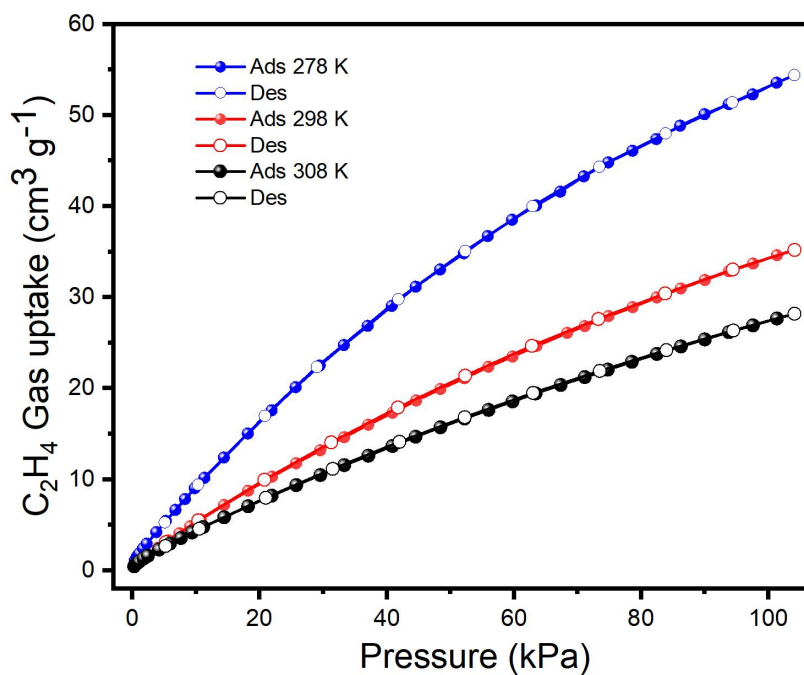
Figure S18. Adsorption and desorption isotherms of C_2H_4 on ZNU-10 at 278 K, 298 K and 308 K.
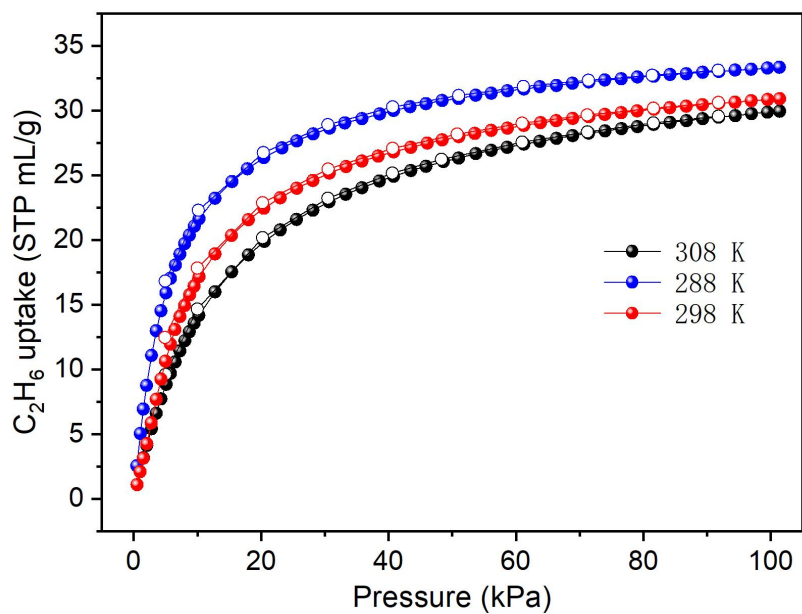
Figure S19. Adsorption and desorption isotherms of C_2H_6 on ZNU-1 under 288, 298 and 308 K.
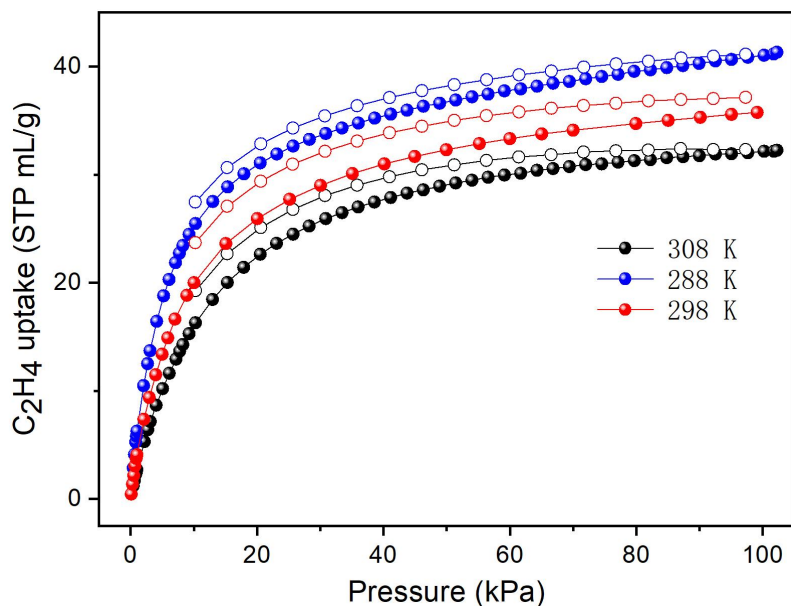
Figure S20. Adsorption and desorption isotherms of C_2H_4 on ZNU-1 under 288, 298 and 308 K.
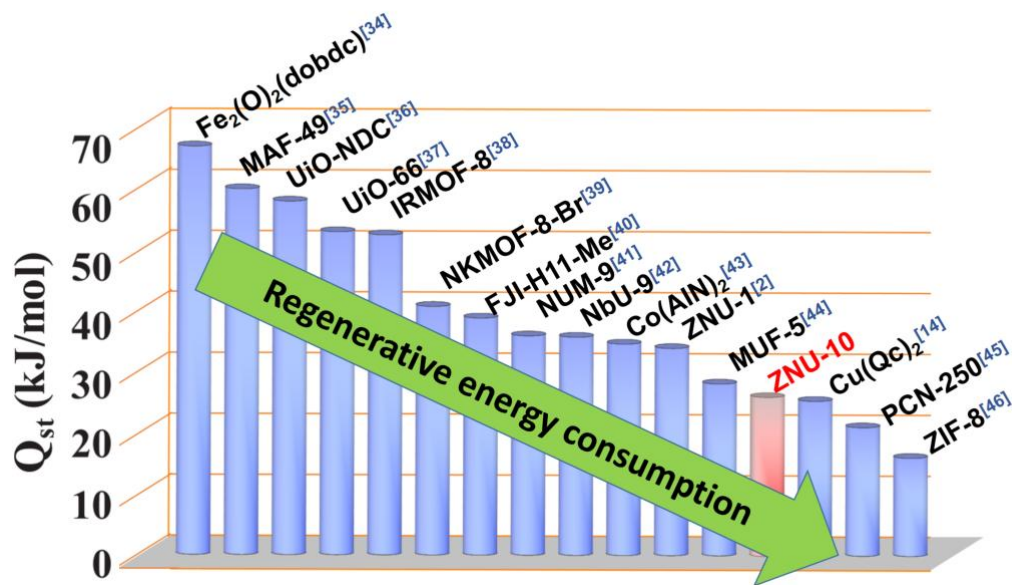
Figure S21. Comparison of the C_2H_6 adsorption heat in some previously reported C_2H_6-selective materials.
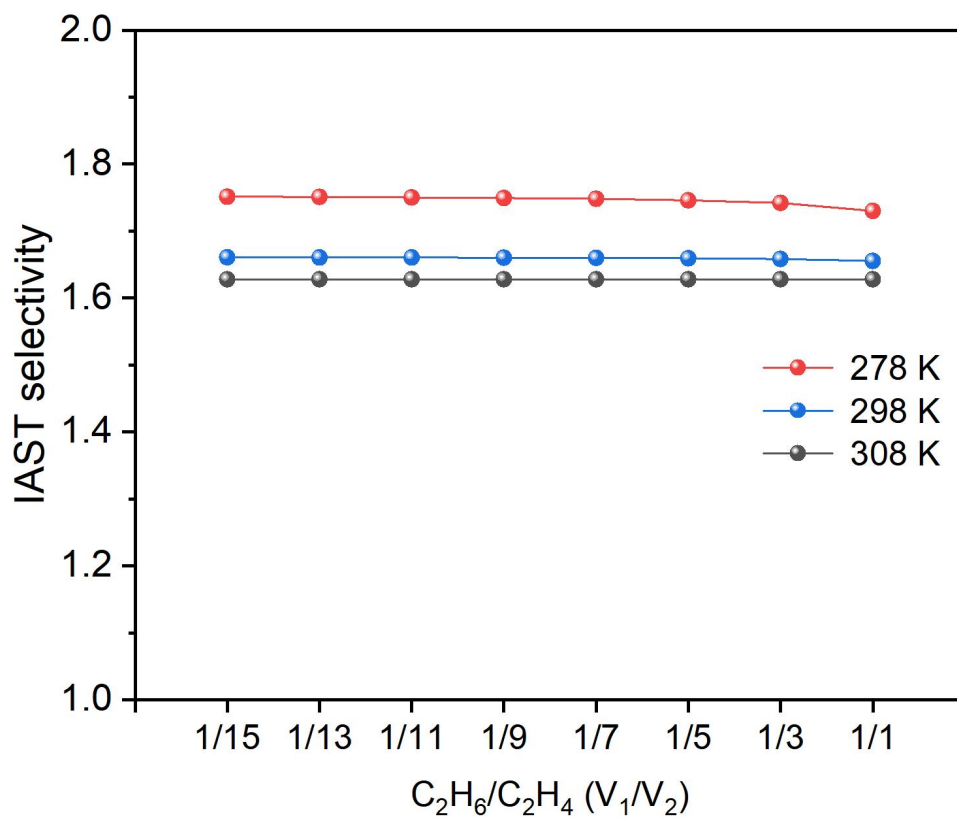
Figure S22. Comparison of the C_2H_6/C_2H_4 selectivity at 100 KPa with different C_2H_6/C_2H_4 ratios under different temperature.

Table S3. Single-site Langmuir parameter fits for C_2H_6 and C_2H_4 adsorption isotherms in ZNU-10.

Gases	q_{sat} L kg^{-1}	b_0 kPa^{-1}	E kJ mol^{-1}	correlation coefficient (R^2)
C_2H_6	101.49	1.95E-07	26.4	0.9995
C_2H_4	114.55	3.67E-07	23.2	0.9997

Table S4. Dual-site or single-site Langmuir parameter fits for C_2H_6 and C_2H_4 adsorption isotherms in ZNU-1 (R^2>0.999).

Gases	$q_{A,sat}$ (mL/g)	b_{A0} (Pa^{-1})	E_A kJ mol^{-1}	$q_{B,sat}$ (mL/g)	b_{B0} (Pa^{-1})	E_B kJ mol^{-1}
C_2H_4	33.6	1.26E-7	34.4	18.82	1.20E-14	65.5
C_2H_6	34.49	1.03E-09	34.10			

Ⅳ Breakthrough experiments

A) Under Work (dry conditions)
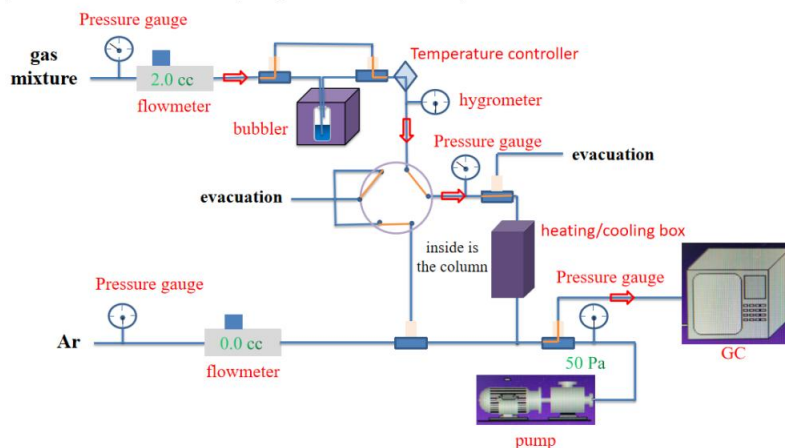
B) Under Work (humid conditions)
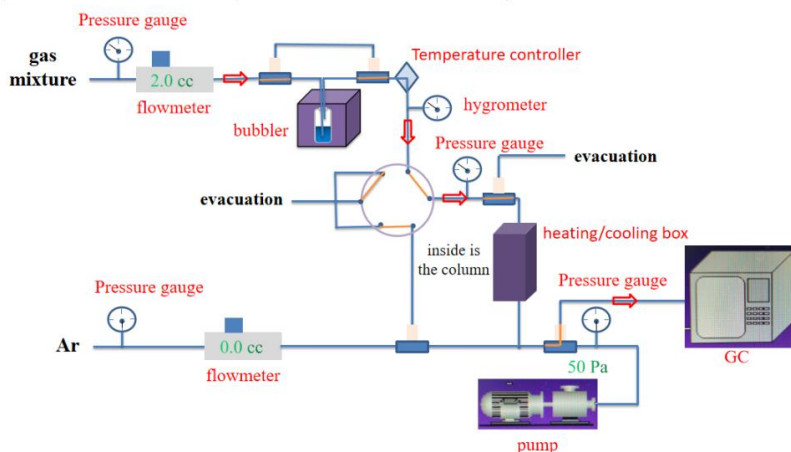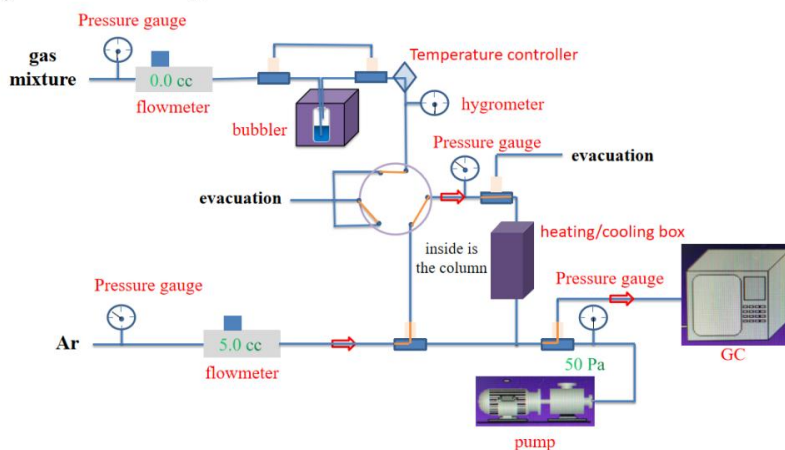
C) Under Purge

Figure S23. The illustration of the gas breakthrough equipment working mechanism containing gas pipelines, pressure gauge, flowmeter, hygrometer, GC, bubbler and pump: A) under work in dry conditions; B) under work in humid conditions; C) under purge.
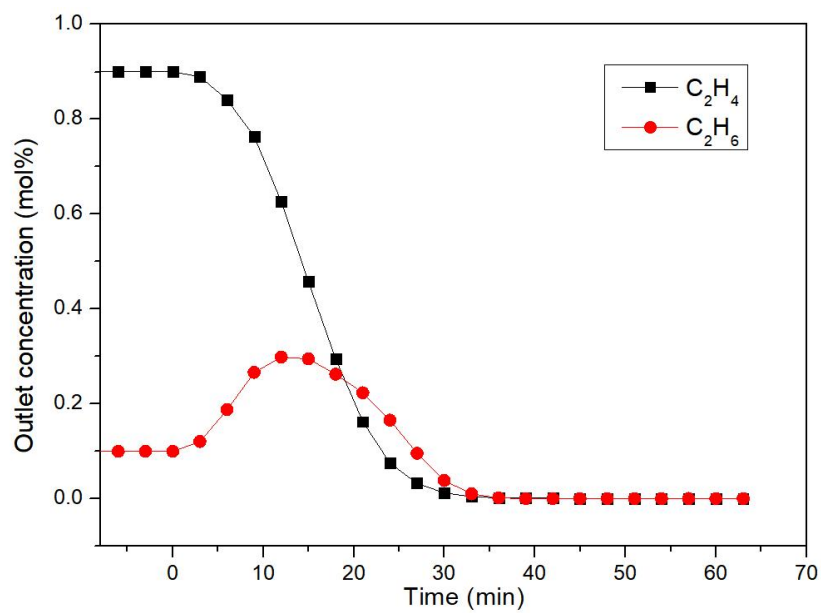
Figure S24. The experimental desorption breakthrough curves of ZNU-10 by Ar purge at 298 K, which indicates that ZNU-10 can be regenerated within 1 h. (Purge begins at T = 0 min)
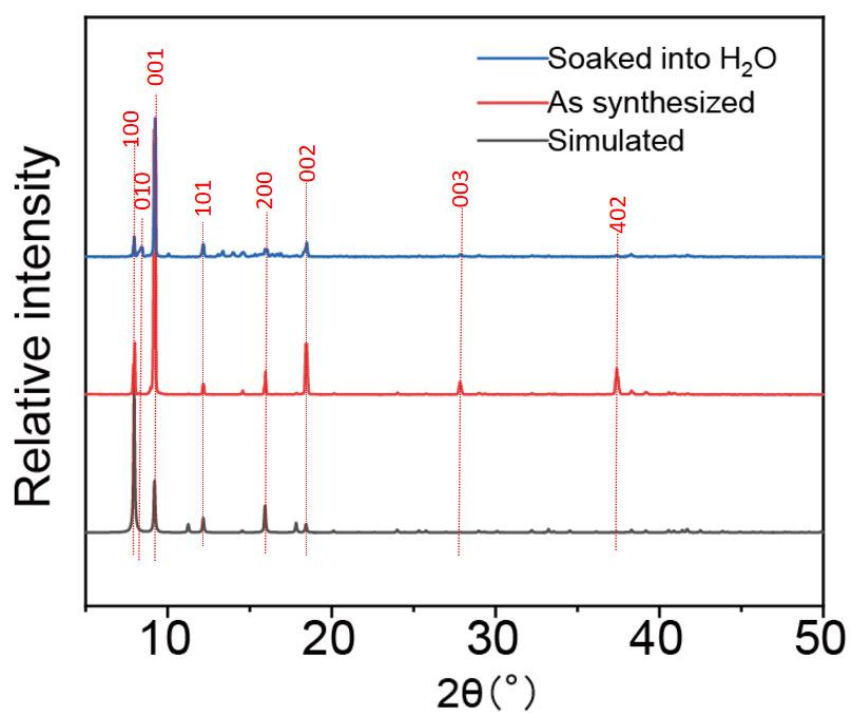
Figure S25. Comparison of the PXRD pattern from simulated ZNU-10, as-synthesized ZNU-10 crystals and ZNU-10 powder after soaking into water for 1 week.
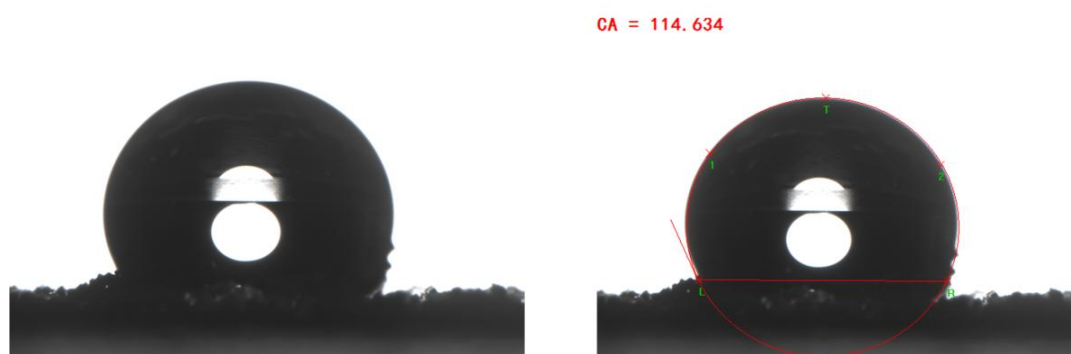
Figure S26. Water contact angle testing of ZNU-10.

Figure S27. Photograph of a drop of water on the crystals of ZNU-10.

V Reference

[1] O. K. Farha, A. M. Spokoyny, K. L. Mulfort, M. F. Hawthorne, C. A. Mirkin and J. T. Hupp, *J. Am. Chem. Soc.* 2007, **129**, 12680-12681.

[2] L. Wang, W. Sun, Y. Zhang, N. Xu, R. Krishna, J. Hu, Y. Jiang, Y. He and H. Xing, *Angew. Chem. Int. Ed.* 2021, **60**, 22865-22870.

[3] J. Pires, J. Fernandes, K. Dedecker, J. R. B. Gomes, G. Pérez-Sánchez, F. Nouar, C. Serre and M. L. Pinto, *ACS Appl. Mater. Interfaces* 2019, **11**, 27410-27421.

[4] B. Zhu, J.-W. Cao, S. Mukherjee, T. Pham, T. Zhang, T. Wang, X. Jiang, K. A. Forrest, M. J. Zaworotko and K.-J. Chen, *J. Am. Chem. Soc.* 2021, **143**, 1485-1492.

[5] Z.-Q. Wang, H.-Q. Luo, Y.-L. Wang, M.-Y. Xu, C.-T. He and Q.-Y. Liu, *Inorg. Chem.* 2021, **60**, 10596-10602.

[6] Y. Chen, H. Wu, D. Lv, R. Shi, Y. Chen, Q. Xia and Z. Li, *Ind. Eng. Chem. Res* 2018, **57**, 4063-4069.

[7] P. Liu, Y. Wang, Y. Chen, J. Yang, X. Wang, L. Li and J. Li, *Sep. Purif. Technol.* 2021, **276**, 119284.

[8] Z. Jiang, L. Fan, P. Zhou, T. Xu, S. Hu, J. Chen, D.-L. Chen and Y. He, *Inorg. Chem. Front.* 2021, **8**, 1243-1252.

[9] M. Kang, S. Yoon, S. Ga, D. W. Kang, S. Han, J. H. Choe, H. Kim, D. W. Kim and Y. G. Chung, C. S. Hong, *Adv. Sci.* 2021, **8**, 2004940.

[10] A. A. Lysova, D. G. Samsonenko, K. A. Kovalenko, A. S. Nizovtsev, D. N. Dybtsev and V. P. Fedin, *Angew. Chem. Int. Ed.* 2020, **59**, 20561-20567.

[11] H. Yang, Y. Wang, R. Krishna, X. Jia, Y. Wang, A. N. Hong, C. Dang, H. E. Castillo, X. Bu and P. Feng, *J. Am. Chem. Soc.* 2020, **142**, 2222-2227.

[12] J. Pei, J.-X. Wang, K. Shao, Y. Yang, Y. Cui, H. Wu, W. Zhou, B. Li and G. Qian, *J. Mater. Chem. A* 2020, **8**, 3613-3620.

[13] X.-W. Gu, J. Pei, K. Shao, H.-M. Wen, B. Li and G. Qian, *ACS Appl. Mater. Interfaces* 2021, **13**, 18792-18799.

[14] R.-B. Lin, H. Wu, L. Li, X.-L. Tang, Z. Li, J. Gao, H. Cui, W. Zhou and B. Chen, *J. Am. Chem. Soc.* 2018, **140**, 12940-12946.

[15] H. Xiang, Y. Shao, A. Ameen, H. Chen, W. Yang, P. Gorgojo, F. R. Siperstein, X. Fan and Q. Pan, *Sep. Purif. Technol.* 2020, **242**, 116819.

[16] H. Xiang, A. Ameen, P. Gorgojo, F. R. Siperstein, S. M. Holmes and X. Fan, *Micropor. Mesopor. Mat.* 2020, **292**, 109724.

[17] X.-W. Lei, H. Yang, Y. Wang, Y. Wang, X. Chen, Y. Xiao, X. Bu and P. Feng, *Small* 2021, **17**, 2003167.

[18] Y. Wang, S. Yuan, Z. Hu, T. Kundu, J. Zhang, S. B. Peh, Y. Cheng, J. Dong, D. Yuan, H.-C. Zhou and D. Zhao, *ACS Sustain. Chem. Eng.* 2019, **7**, 7118-7126.

[19] Z. Xu, X. Xiong, J. Xiong, R. Krishna, L. Li, Y. Fan, F. Luo and B. Chen, *Nat. Chem.* 2020, **11**, 3163.

[20] A. Schneemann, Y. Jing, J. D. Evans, T. Toyao, Y. Hijikata, Y. Kamiya, K.-i. Shimizu, N. C. Burtch and S.-i. Noro, *Dalton Trans.* 2021, **50**, 10423-10435.

[21] H. Wu, Y. Chen, W. Yang, D. Lv, Y. Yuan, Z. Qiao, H. Liang, Z. Li and Q. Xia, *Industrial & Ind. Eng. Chem. Res* 2019, **58**, 10516-10523.

[22] J. Liu, J. Miao, S. Ullah, K. Zhou, L. Yu, H. Wang, Y. Wang, T. Thonhauser and J. Li, *ACS Mater. Lett.* 2022, **4**, 1227-1232.

[23] C.-X. Chen, Z.-W. Wei, T. Pham, P. C. Lan, L. Zhang, K. A. Forrest, S. Chen, A. M. Al-Enizi, A. Nafady, C.-Y. Su and S. Ma, *Angew. Chem. Int. Ed.* 2021, **60**, 9680-9685.

[24] L. Wang, N. Xu, Y. Hu, W. Sun, R. Krishna, J. Li, Y. Jiang, S. Duttwyler and Y. Zhang, *Nano Res.* 2023, **16**, 3536-3541.

[25] Y. Jiang, J. Hu, L. Wang, W. Sun, N. Xu, R. Krishna, S. Duttwyler, X. Cui, H. Xing and Y. Zhang, *Angew. Chem. Int. Ed.* 2022, **61**, e202200947.

[26] W.-Q. Sun, J.-B. Hu, Y.-J. Jiang, N. Xu, L.-Y. Wang, J.-H. Li, Y.-Q. Hu, S. Duttwyler and Y.-B. Zhang, *Chem. Eng. J.* 2022, **439**, 135745.

[27] Y. Zhang, J. Hu, R. Krishna, L. Wang, L. Yang, X. Cui, S. Duttwyler and H. Xing, *Angew. Chem. Int. Ed.* 2020, **59**, 17664-17669.

[28] N. Xu, T. Yan, J. Li, L. Wang, D. Liu and Y. Zhang, *Inorg. Chem. Front.* 2023, **10**, 522-528.

[29] Y. Jiang, Y. Hu, B. Luan, L. Wang, R. Krishna, H. Ni, X. Hu and Y. Zhang, *Nat. Chem.* 2023, **14**, 401.

[30] N. Xu, J. Hu, L. Wang, D. Luo, W. Sun, Y. Hu, D. Wang, X. Cui, H. Xing and Y. Zhang, *Chem. Eng. J.* 2022, **450**, 138034.

[31] Y. Zhang, W. Sun, B. Luan, J. Li, D. Luo, Y. Jiang, L. Wang and B. Chen, *Angew. Chem. Int. Ed.* 2023, **n/a**, e202309925.

[32] Y. Zhang, L. Yang, L. Wang, S. Duttwyler and H. Xing, *Angew. Chem. Int. Ed.*

2019, **58**, 8145-8150.

[33] Y. Zhang, L. Yang, L. Wang, X. Cui and H. Xing, *J. Mater. Chem. A* 2019, **7**, 27560-27566.

[34] L. Li, R.-B. Lin, R. Krishna, H. Li, S. Xiang, H. Wu, J. Li, W. Zhou and B. Chen, *Science* 2018, **362**, 443-446.

[35] P.-Q. Liao, W.-X. Zhang, J.-P. Zhang and X.-M. Chen, *Nat. Chem.* 2015, **6**, 8697.

[36] J. Pires, J. Fernandes, K. Dedecker, J. R. B. G. Gomes, Pérez-Sánchez, F. Nouar, C. Serre and M. L. Pinto, *ACS Appl. Mater. Interfaces* 2019, **11**, 27410-27421.

[37] L. Valenzano, B. Civalleri, S. Chavan, S. Bordiga, M. H. Nilsen, S. Jakobsen, K. P. Lillerud and C. Lamberti, *Chem. Mater.* 2011, **23**, 1700-1718.

[38] J. I. Feldblyum, A. G. Wong-Foy and A. J. Matzger, *Chem. Mater.* 2012, **48**, 9828-9830.

[39] P. Guo, Y. Chen, M. Chang, Y. Li, Q. Yang and D. Liu, *J. Chem. Eng. Data* 2022, **67**, 1654-1662.

[40] Z. Di, C. Liu, J. Pang, S. Zou, Z. Ji, F. Hu, C. Chen, D. Yuan, M. Hong and M. Wu, *Angew. Chem. Int. Ed.* 2022, **61**, e202210343.

[41] S.-Q. Yang, F.-Z. Sun, P. Liu, L. Li, R. Krishna, Y.-H. Zhang, Q. Li, L. Zhou and T.-L. Hu, *ACS Appl. Mater. Interfaces* 2021, **13**, 962-969.

[42] J. Li, S. Chen, L. Jiang, D. Wu and Y. Li, *Inorg. Chem.* 2019, **58**, 5410-5413.

[43] S. Jiang, L. Li, L. Guo, C. Song, Q. Yang, Z. Zhang, Y. Yang, Q. Ren and Z. Bao, *Sci. China Chem.* 2021, **64**, 666-672.

[44] O. T. Qazvini, R. Babarao, Z.-L. Shi, Y.-B. Zhang and S. G. Telfer, *J. Am. Chem.*

Soc. 2019, **141**, 5014-5020.

[45] Y. Chen, Z. Qiao, H. Wu, D. Lv, R. Shi, Q. Xia, J. Zhou and Z. Li, *Sci. China. Chem.* 2018, **175**, 110-117.

[46] U. Böhme, B. Barth, C. Paula, A. Kuhnt, W. Schwieger, A. Mundstock, J. Caro and M. Hartmann, 2013, **29**, 8592-8600.